



RESEARCH ARTICLE

Double delay alternating with nutation for tailored excitation facilitates banding-free isotropic high-resolution intracranial vessel wall imaging

Bram F. Coolen¹ | Jasper Schoormans¹ | Guillaume Gilbert² |
Ernst S. Kooreman^{1,3} | Naomi de Winter¹ | Olivia Viessmann⁴ |
Jaco J. M. Zwanenburg⁵  | Charles B. L. M. Majoie⁶ | Gustav J. Strijkers¹ |
Aart J. Nederveen⁶ | Jeroen C. W. Siero^{5,7} 

¹Department of Biomedical Engineering & Physics, Amsterdam UMC, Amsterdam, The Netherlands

²MR Clinical Science, Philips Canada, Markham, Ontario, Canada

³Department of Radiation Oncology, The Netherlands Cancer Institute, Amsterdam, The Netherlands

⁴Athinoula A. Martinos Center for Biomedical Imaging, Department of Radiology, Harvard Medical School, Massachusetts General Hospital, Charlestown, Massachusetts, USA

⁵Department of Radiology, University Medical Center Utrecht, Utrecht University, Utrecht, The Netherlands

⁶Department of Radiology & Nuclear Medicine, Amsterdam UMC, Amsterdam, The Netherlands

⁷Spinoza Centre for Neuroimaging, Amsterdam, The Netherlands

Correspondence

Bram F. Coolen, Amsterdam UMC,
Department of Biomedical Engineering &
Physics Meibergdreef 9, 1105 AZ, Amsterdam
The Netherlands.

Email: b.f.coolen@amsterdamumc.nl

Funding information

Dutch Research Council, Grant/Award
Number: 14348

The purpose of this study was to evaluate the use of a double delay alternating with nutation for tailored excitation (D-DANTE)-prepared sequence for banding-free isotropic high-resolution intracranial vessel wall imaging (IC-VWI) and to compare its performance with regular DANTE in terms of signal-to-noise ratio (SNR) as well as cerebrospinal fluid (CSF) and blood suppression efficiency. To this end, a D-DANTE-prepared 3D turbo spin echo sequence was implemented by interleaving two separate DANTE pulse trains with different RF phase-cycling schemes, but keeping all other DANTE parameters unchanged, including the total number of pulses and total preparation time. This achieved a reduction of the banding distance compared with regular DANTE enabling banding-free imaging up to higher resolutions. Bloch simulations assuming static vessel wall and flowing CSF spins were performed to compare DANTE and D-DANTE in terms of SNR and vessel wall/CSF contrast. Similar image quality measures were assessed from measurements on 13 healthy middle-aged volunteers. Both simulation and in vivo results showed that D-DANTE had only slightly lower vessel wall/CSF and vessel wall/blood contrast-to-noise ratio values compared with regular DANTE, which originated from a 10%–15% reduction in vessel wall SNR but

Abbreviations used: BA, basilar artery; CSF, cerebrospinal fluid; DANTE, delay alternating with nutation for tailored excitation; D-DANTE, Double DANTE; IC-VWI, intracranial vessel wall imaging; MCA, middle cerebral artery; MSDE, motion-sensitized driven equilibrium; SENSE, sensitivity encoding; SSFP, steady-state free precession; TSE, turbo spin echo; VW, vessel wall.

Bram F. Coolen and Jasper Schoormans contributed equally to this study.

This is an open access article under the terms of the Creative Commons Attribution-NonCommercial License, which permits use, distribution and reproduction in any medium, provided the original work is properly cited and is not used for commercial purposes.

© 2021 The Authors. *NMR in Biomedicine* published by John Wiley & Sons Ltd.

not from reduced CSF or blood suppression efficiency. As anticipated, IC-VWI acquisitions showed that D-DANTE can successfully remove banding artifacts compared with regular DANTE with equal scan time or DANTE preparation length. Moreover, application was demonstrated in a patient with an intracranial aneurysm, indicating improved robustness to slow flow artifacts compared with clinically available 3D turbo spin echo scans. In conclusion, D-DANTE provides banding artifact-free IC-VWI up to higher isotropic resolutions compared with regular DANTE. This allows for a more flexible choice of DANTE preparation parameters in high-resolution IC-VWI protocols.

KEYWORDS

atherosclerosis, CSF suppression, DANTE, intracranial vessel wall imaging

1 | INTRODUCTION

Intracranial vessel wall imaging (IC-VWI) has been shown to be a powerful tool with which to identify and characterize atherosclerotic plaques in major brain-feeding arteries around the circle of Willis, such as the basilar, middle and anterior/posterior cerebral arteries. The application of IC-VWI has become increasingly feasible since the introduction of 3D variable refocusing angle turbo spin echo (TSE) imaging sequences, which provide both the inherent blood suppression and high isotropic resolution imaging necessary to delineate the thin intracranial vessel wall (VW).^{1,2} One major challenge for IC-VWI, however, is the remaining signal from the cerebrospinal fluid (CSF), which compromises qualitative and quantitative evaluation of the intracranial vessels directly in contact with CSF. A straightforward solution to suppress CSF signal is the use of fluid-attenuated inversion recovery (FLAIR) preparation, but this sequence has low signal-to-noise ratio (SNR) efficiency, and achieving the required spatial resolution in a reasonable acquisition time is therefore only feasible at high field strength (7T) in combination with high parallel imaging factors.³ At clinical 3T, CSF suppression can be achieved more efficiently by means of additional flow-sensitive prepulses. Two possible types of prepulses have been proposed in the literature, motion-sensitized driven equilibrium (MSDE)⁴ and delay alternating with nutation for tailored excitation (DANTE),⁵ which are also commonly used for blood suppression in various other vascular beds.^{6,7} DANTE, as opposed to MSDE, also has highly effective flow suppression up to very slow velocities of less than 1 cm/s,⁵ which is very advantageous to obtain adequate CSF suppression. This explains the increasing use of DANTE for IC-VWI applications.⁸⁻¹⁰

An important property of the DANTE prepulse is the periodically changing signal amplitude as a function of the off-resonance frequency, similar to what has been described for steady-state free precession (SSFP) sequences.¹¹ While this has been exploited successfully in MR tagging applications,¹² this is obviously an undesired phenomenon in IC-VWI because of possible banding artifacts across the image, which occur if the banding separation Δr is not small enough compared with the voxel dimension along the DANTE gradient direction. More specifically, Δr is directly related to the DANTE pulse interval τ and gradient strength G as follows:

$$\Delta r = \frac{2\pi}{\tau \gamma G}. \quad (1)$$

Whereas increasing τ compromises the duration of the DANTE prepulse or efficiency of flow suppression,⁹ an increase in G might also be compromised by hardware limitations, restrictions related to peripheral nerve stimulation and intolerable acoustic noise levels. This may compromise DANTE in achieving isotropic high-resolution IC-VWI, which is needed because of the thin wall and strong tortuosity of the intracranial arteries. To increase the flexibility in DANTE preparation, we here propose the use of a different type of DANTE preparation, called "Double DANTE" (D-DANTE).^{13,14} D-DANTE can reduce the banding separation without changes in the DANTE pulse train length or any of the DANTE parameters, except for the specific phase-cycling scheme employed. In this study, we aimed to compare the performance of DANTE and D-DANTE in terms of SNR as well as CSF and blood suppression efficiency through simulations and a feasibility study in healthy volunteers.

2 | METHODS

2.1 | DANTE versus D-DANTE

Figure 1A shows the sequence designs for both DANTE and D-DANTE preparation. In general, DANTE preparation consists of alternating RF and gradient pulse trains, causing a tagged-like pattern across the field of view (FOV) (Figure 1B). Regular DANTE is generally performed with RF

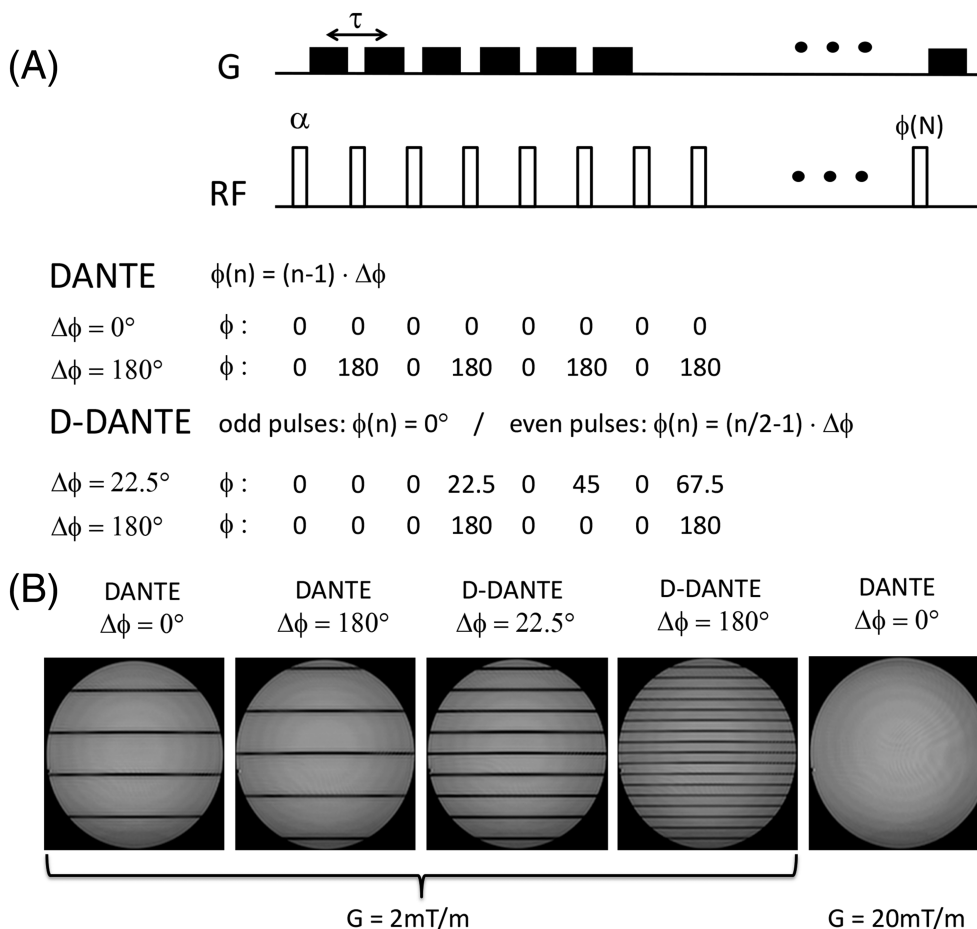


FIGURE 1 (A) DANTE and D-DANTE preparations, both consisting of a pulse train with flip angle α , RF pulse interval τ , combined with gradients with strength G during each interval. Whereas DANTE has a regular phase increment ($\Delta\Phi$) for each pulse, which is generally 0° or 180° , D-DANTE has two interleaved pulse trains with $\Delta\Phi = 0^\circ$ for uneven RF pulses and $\Delta\Phi > 0^\circ$ for even RF pulses. This produces distinct phase evolutions between DANTE and D-DANTE, as can be seen from the examples provided. (B) DANTE ($\Delta\Phi = 0^\circ$ or $\Delta\Phi = 180^\circ$) and D-DANTE ($\Delta\Phi = 22.5^\circ$ or $\Delta\Phi = 180^\circ$) acquisitions in a cylindrical phantom. Whereas for regular DANTE applying a different phase increment only shifts the location of the bands, with D-DANTE additional bands are created, of which the exact distribution depends on the choice of $\Delta\Phi$. For this particular purpose, the gradient strength was chosen to be very low (2 mT/m) to accentuate the banding effect. An acquisition with a higher gradient is shown as well, which is needed in practice to decrease banding distance below the voxel dimensions. DANTE, delay alternating with nutation for tailored excitation; D-DANTE, Double DANTE

phase increment values of $\Delta\Phi = 0^\circ$ or $\Delta\Phi = 180^\circ$,⁵ which effectively only differ in the location of the signal bands, as described in detail by Bernstein et al.¹⁴ Conversely, D-DANTE has two interleaved pulse trains, with $\Delta\Phi = 0^\circ$ for odd RF pulses and $\Delta\Phi > 0^\circ$ for even RF pulses. Because each individual pulse train then effectively has a pulse interval 2τ (Equation 1), it can be shown that for D-DANTE the banding separation is decreased by a factor of 2, even for small values of $\Delta\Phi$, and even by a factor of 4 when choosing $\Delta\Phi = 180^\circ$ (Figure 1B). This is also clear from Bloch simulations of the D-DANTE frequency response, as shown in Figure S1. Notably, the total number of pulses (N) as well as the actual inter-pulse time τ remain equal to that of regular DANTE, thereby not increasing the total DANTE pulse train length. This means that, regardless of the DANTE preparation parameters, D-DANTE allows for a higher spatial resolution compared with regular DANTE before the appearance of banding artifacts would occur.

2.2 | Simulations assuming CSF flow

To compare DANTE and D-DANTE in terms of CSF suppression, Bloch simulations were performed in MATLAB2017b (MathWorks, Natick, MA, USA), similar to Viessmann et al.,¹⁰ using an ensemble of 1000 individual spins. For CSF, a linear velocity profile within a simulated voxel of 0.8 mm was assumed with a velocity distribution of 2 cm/s \pm 10%. Relaxation parameters of CSF and VW tissues were assumed as follows: $T_{1\text{CSF}} = 4000$ ms, $T_{2\text{CSF}} = 2000$ ms, $T_{1\text{VW}} = 1000$ ms, $T_{2\text{VW}} = 55$ ms.^{15–20} Based on earlier optimizations,²¹ DANTE parameters in simulations

as well as in the volunteer study were chosen as follows: $\alpha = 8^\circ$, $N = 300$, $\tau = 1$ ms, $G = 22.5$ mT/m (three directions). DANTE was performed with $\Delta\Phi = 0^\circ$, whereas for D-DANTE, $\Delta\Phi$ was either 22.5° or 180° . An example of such a simulation showing the saturation of longitudinal magnetization by DANTE preparation can be found in the supporting information (Video S1).

2.3 | Feasibility study

All experiments in this study adhered to the guidelines of the local Medical Ethical Committee and were performed in accordance with the declaration of Helsinki. All participants provided written informed consent prior to the start of the study. DANTE and D-DANTE were implemented on a 3-T Philips Ingenia CX MRI scanner. To assess differences in contrast-to-noise ratio (CNR) and flow suppression efficiency between DANTE and D-DANTE in vivo, 13 healthy middle-aged volunteers (seven males, six females; age 58 ± 8 years) were scanned. After scout scans of the brain, phase-contrast angiography was performed for visualization of the main intracranial arteries. Subsequently, DANTE/D-DANTE-prepared variable refocusing angle TSE sequences were performed in the region covering the circle of Willis at a moderate angulation (25° – 35°) with respect to the AC-PC line. Because pilot measurements revealed that regular DANTE produced banding artifacts at 0.6-mm isotropic resolution (also see Discussion), we used a more conservative resolution of 0.8 mm to ensure accurate VW delineation and comparison between the two DANTE preparations in terms of flow suppression. Next to these scans, an additional D-DANTE acquisition at a higher isotropic resolution of 0.6 mm was performed. All DANTE-prepared scans were performed in random order. To clarify, we used the same gradient strength of 22.5 mT/m in all directions, which means the effective gradient is $\sqrt{3} * 22.5 = 39$ mT/m. Because of the isotropic voxel size, the minimum banding distance Δr is then equal to $1/(42.57 * 39 * 0.001) = 0.6$ mm for regular DANTE and 0.3 mm for D-DANTE. As the banding distance needs to be significantly smaller than the voxel size to effectively average out the frequency-dependent signal response within each voxel, banding artifacts occur for regular DANTE at 0.6-mm isotropic resolution using our DANTE settings, but not at 0.8-mm isotropic resolution. By contrast, when applying D-DANTE, both resolutions do not show any banding artifacts. Other DANTE parameters were as described in the simulations (see above), except that only $\Delta\Phi = 22.5^\circ$ was used for D-DANTE. Other TSE readout parameters were as follows: TR/TE = 1500/46 ms, refocusing pulse train = 40° – 120° , TSE factor = 56, interecho time = 4.5 ms, startup echoes = 6, FOV = $200 \times 180 \times 60$ mm³, SENSE factor (A-P) = 2, profile order = radial, elliptical k-space shutter = yes. Acquisition times were 3 min 30 s and 5 min 46 s (excluding additional noise scans) for 0.8-mm and 0.6-mm isotropic scans, respectively.

To correctly assess noise in the region of interest (ROI), which may be affected by SENSE-related noise amplification, each scan was followed by a “noise-specific” scan, which was implemented as a second dynamic scan but with RF and gradients turned off (and reduced dead times to minimize acquisition time). In addition to the experiments with healthy volunteers, a high-resolution D-DANTE scan was performed in a clinical setting in a patient with a known intracranial aneurysm.

2.4 | Image analysis and statistics

For comparison of DANTE and D-DANTE scans, signal intensities (S) of VW, lumen and CSF were assessed both at the middle cerebral artery (MCA) and basilar artery (BA) locations in the 0.8-mm isotropic resolution scans. For each of the arteries, segmentation of different tissue ROIs was performed in ITK-SNAP²² in at least five slices where the arteries were clearly visible. Segmentations at the different slice locations were considered as one large ROI, from which the mean signal intensity value was calculated. Mean noise (N) values for each scan were extracted from the additional noise scans (see above) using circular ROIs representing an area with homogenous noise amplitude covering the overall imaging ROI. Because the reconstruction procedure of the noise scan is identical to its preceding scan, this allows direct noise measurements at the same region for which the tissue signal measurements are taken, avoiding the need for alternative techniques as proposed by Kellman and McVeigh.²³ Because noise values were calculated from magnitude noise images, SNR within each ROI was defined as $1.25 * S/N$,²⁴ assuming a the Rayleigh distribution of noise values. Similarly, CNR between tissues was calculated as $1.25 * (S_{\text{tissue1}} - S_{\text{tissue2}}) / N$.

Differences in SNR and CNR between DANTE and D-DANTE were assessed using repeated-measures ANOVA with vessel type (BA/MCA) and DANTE type as within-subject factors. The level of statistical significance was set at $p = 0.05$.

3 | RESULTS

Simulation results in Figure 2 show the evolution of longitudinal magnetization (M_z) during the 300-ms DANTE preparation. As expected, regular DANTE preserves most of the VW (M_z) magnetization at the end of preparation ($0.88 M_0$), whereas for D-DANTE an additional signal loss was observed to a value of $0.76 M_0$ as a result of the increased number of signal modulation bands and therefore lower overall voxel intensity. More importantly, because suppression of flowing CSF remains effective for D-DANTE, VW/CSF contrast (fraction of M_0) is affected to a similar degree

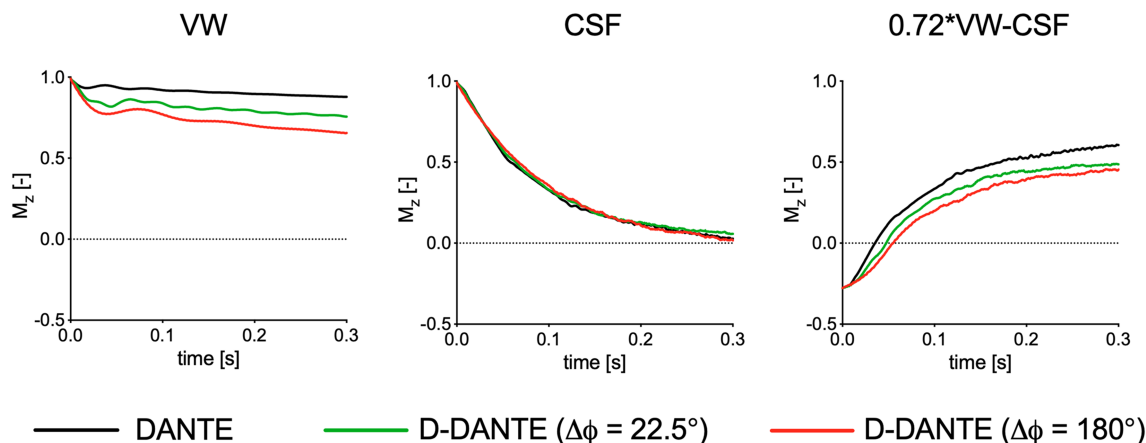


FIGURE 2 Bloch simulations of vessel wall (VW) and cerebrospinal fluid (CSF) longitudinal magnetization evolution during DANTE (black) and D-DANTE preparations with either $\Delta\Phi = 22.5^\circ$ (green) or $\Delta\Phi = 180^\circ$ (red). Simulations were performed using an ensemble of 1000 spins at different positions along the DANTE gradient. A linear velocity profile across the voxel was assumed for CSF tissue. To calculate VW/CSF contrast, the proton density ratio was assumed to be 0.72.¹⁰ DANTE, delay alternating with nutation for tailored excitation; D-DANTE, Double DANTE

compared with regular DANTE ($0.6 * M_0$), with a slightly better performance for $\Delta\Phi = 22.5^\circ$ ($0.49 * M_0$) compared with $\Delta\Phi = 180^\circ$ ($0.45 * M_0$). For the current sequence parameters, VW/CSF contrast plateaued towards the end of the preparation time.

Figure 3A and 3B show representative examples of DANTE and D-DANTE scans as well as representative BA and MCA segmentations of the same volunteer. In both cases, adequate CSF suppression and delineation of the vessel wall can be appreciated. Table 1 contains quantitative results comparing SNR and CNR calculated for different ROIs. In line with simulations, in vivo results show D-DANTE slightly compromises VW/CSF as well as VW/lumen CNR values for both BA and MCA regions. This predominantly seems to originate from a reduced SNR within the VW, rather than a reduction in CSF and/or blood suppression. The reduction in SNR as measured in VW (11% for both BA and MCA regions) is close to simulated values (14%), as well as that of the brain tissue reference region (14%). There was no significant interaction between the type of DANTE preparation (DANTE vs. D-DANTE) and artery location (BA vs. MCA). For both DANTE types, MCA regions showed slightly higher VW SNR, but also slightly worse CSF suppression compared with the BA region, which resulted in similar VW/CSF CNR values. By contrast, VW/lumen CNR seemed slightly higher for MCA than BA regions.

When applying VWI at 0.6-mm isotropic resolution (Figure 4), banding artifacts were noticed for regular DANTE, compromising image quality and VW delineation. On the other hand, D-DANTE showed no banding and clear delineation of all major intracranial arteries. VW/CSF CNR (BA: 4.3; MCA: 4.1) and VW/lumen CNR (BA: 4.3; MCA: 4.1) were 45%–50% lower compared with values at 0.8-mm isotropic resolution, which corresponds well with the expected SNR loss solely based on voxel size.

As an additional clinical feasibility test, we scanned a patient with a known cerebral aneurysm in the left MCA using 0.6-mm isotropic D-DANTE (Figure 5). The aneurysm wall can clearly be seen using our new method. Moreover, when comparing D-DANTE with a regular TSE, which was part of the clinical research protocol, postcontrast scans without DANTE showed regional enhancement in the MCA, as well as around small peripheral brain vessels, whereas these enhancement patterns were absent for the D-DANTE scans. Upon closer inspection of the vessel structures, the enhancement at the MCA was proven to originate from a crossing vein, for which the slow-flowing blood was only suppressed by D-DANTE.

4 | DISCUSSION

IC-VWI has quickly gained interest in recent years, especially because it has allowed a detailed evaluation of intracranial artery plaques as an alternative source of stroke when no plaque or stenosis is found in the carotids. The need for isotropic high-resolution imaging in this application arises from the VW being thin and from the strong tortuosity of the arteries. In addition, adequate CSF suppression is needed to achieve sufficient VW visibility and delineation. Although some studies have already demonstrated the superiority of 3D DANTE compared with normal 3D TSE in terms of VW/CSF contrast,^{10,21} the banding artifact problem of DANTE is generally understated²⁵ and often mitigated by using isotropic voxels at moderate resolution,⁸ anisotropic voxels²¹ or either high DANTE gradients or RF pulse intervals.²⁶ In this study, we have demonstrated an alternative “double-DANTE” preparation, D-DANTE, which prevents banding artifacts at high isotropic resolution with only small compromises in VW/CSF and VW/lumen contrast.

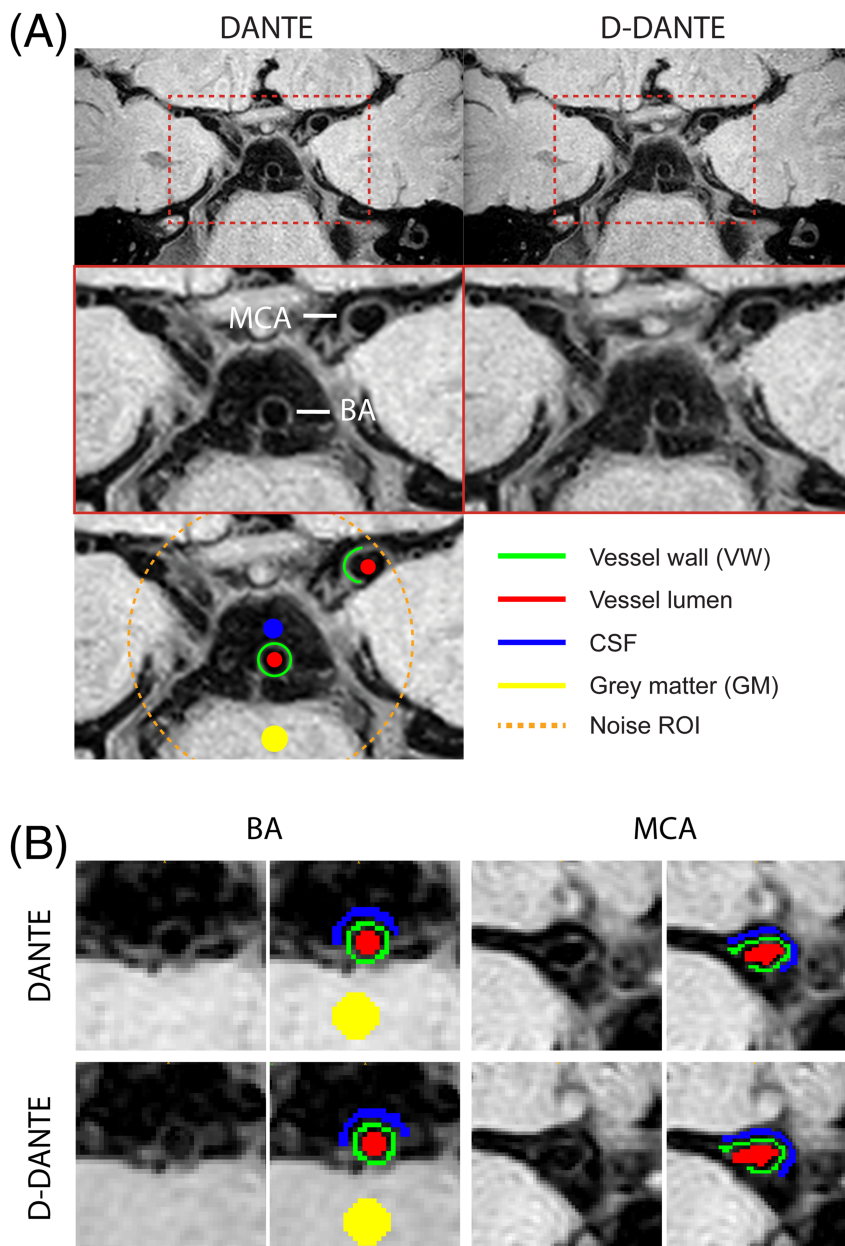


FIGURE 3 (A) Representative DANTE and D-DANTE intracranial vessel wall imaging (IC-VWI) scans at 0.8-mm isotropic resolution. The basilar artery (BA) and middle cerebral artery (MCA) are indicated. Schematic regions of interest (ROIs) (green = vessel wall [VW]; blue = cerebrospinal fluid [CSF]; red = blood) used for quantitative comparisons in image quality between the different IC-VWI sequences are indicated. The orange line indicates the region from which noise was calculated from the additional noise scan. Additionally, a reference region (yellow) was drawn in the pons, which was the most proximal brain tissue region. (B) Representative segmentation ROIs for one volunteer as drawn in ITK-SNAP for DANTE and D-DANTE scans. DANTE, delay alternating with nutation for tailored excitation; D-DANTE, Double DANTE; GM, gray matter

The maximum resolution we used was 0.6-mm isotropic, which clearly showed banding artifacts for regular DANTE but not for D-DANTE. Therefore, to ensure accurate VW delineation and comparison between the two DANTE preparations in terms of flow suppression, we chose a conservative resolution of 0.8-mm isotropic. Besides the possibility of achieving higher spatial resolution without banding, the application of D-DANTE in general, and also for extracranial arteries, will allow more flexibility in choosing the gradient strength and pulse interval τ , in case gradient strength is limited or to mitigate high acoustic noise levels commonly associated with DANTE at specific values for τ . Examples of high-resolution (0.5–0.6 mm) imaging using regular DANTE have been reported in the literature.^{8,9,27} One reason for the small discrepancy between our study and others regarding the exact resolution at which banding occurs is that our DANTE sequence implementation probably did not lead to the absolute maximum gradient moment possible during the DANTE pulse interval. Note that this does not change the fact that D-DANTE will

TABLE 1 Quantitative results comparing signal-to-noise ratio (SNR) and contrast-to-noise ratio (CNR) outcome measures between DANTE and D-DANTE scans at 0.8-mm isotropic resolution

			DANTE	D-DANTE	<i>p</i> value
CNR	VW/CSF	BA	9.0 +/- 2.2	7.9 +/- 2.2	<0.01
		MCA	9.7 +/- 2.1	8.8 +/- 1.9	<0.01
	VW/lumen	BA	8.9 +/- 2.4	8.0 +/- 2.4	0.03
		MCA	12.9 +/- 1.9	11.1 +/- 1.2	<0.01
SNR	Vessel wall	BA	12.5 +/- 3.0	11.1 +/- 2.5	0.01
		MCA	16.5 +/- 2.1	14.6 +/- 1.3	<0.01
	CSF	BA	3.4 +/- 1.6	3.3 +/- 1.2	0.58
		MCA	6.8 +/- 2.5	5.8 +/- 2.0	0.03
	Lumen	BA	3.6 +/- 0.8	3.2 +/- 0.7	0.18
		MCA	3.6 +/- 0.5	3.5 +/- 0.7	0.66
GM	-	30.8 +/- 2.6	26.6 +/- 2.6	<0.01	

Note: Resulting *p* values from post hoc paired *t*-tests. Statistically significant results are indicated in bold. Abbreviations: BA, basilar artery; CSF, cerebrospinal fluid; DANTE, delay alternating with nutation for tailored excitation; D-DANTE, Double DANTE; GM, gray matter; MCA, middle cerebral artery; VW, vessel wall.

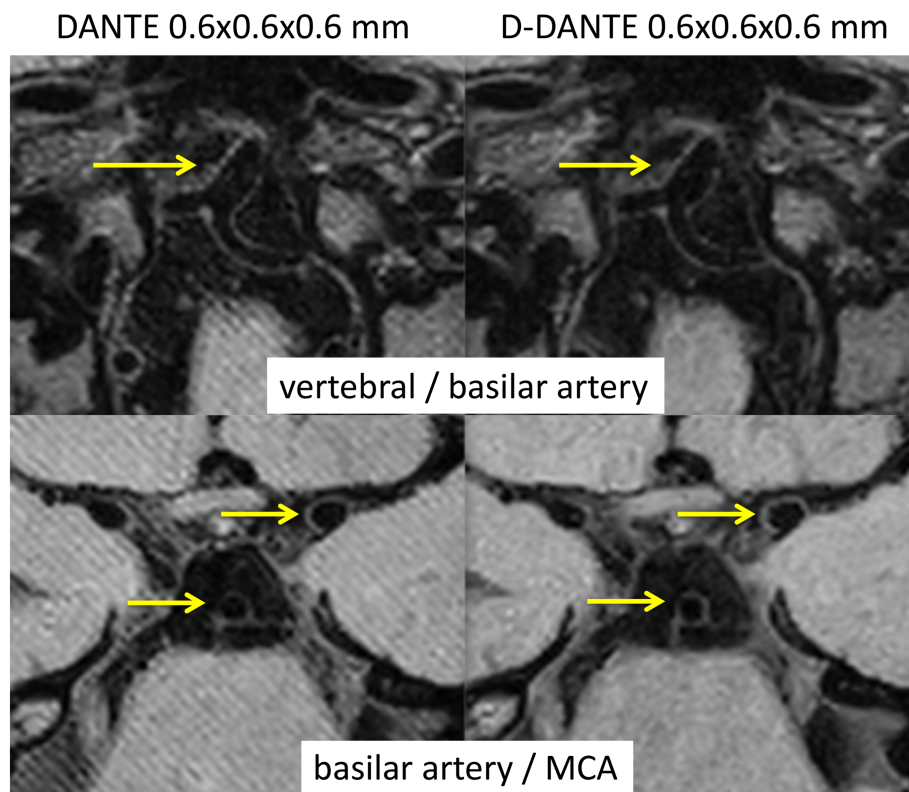


FIGURE 4 DANTE and D-DANTE imaging at 0.6-mm isotropic resolution. Whereas for regular DANTE scans banding artifacts compromise image quality and vessel wall delineation, D-DANTE scans using the same imaging parameters do not suffer from these artifacts. DANTE, delay alternating with nutation for tailored excitation; D-DANTE, Double DANTE; MCA, middle cerebral artery

always lead to less banding than regular DANTE for equivalent parameters, which is the main conclusion of the current study. Other reasons for the absence of banding in the literature might be a mismatch between acquired and reconstructed resolution, or that banding occurs in the slice-selection direction and is therefore not apparent on individual images of the 3D volume. Finally, other researchers have performed IC-VWI without DANTE at higher resolutions of up to 0.4-mm isotropic,^{28–31} which naturally compromises imaging time and SNR. An increase in resolution affects the 3D TSE readout and total acquisition time, but not the DANTE preparation itself. Because the main objective of this study was to assess the added value of D-DANTE compared with regular DANTE by exact comparison of the two sequences, the 3D TSE readout may be

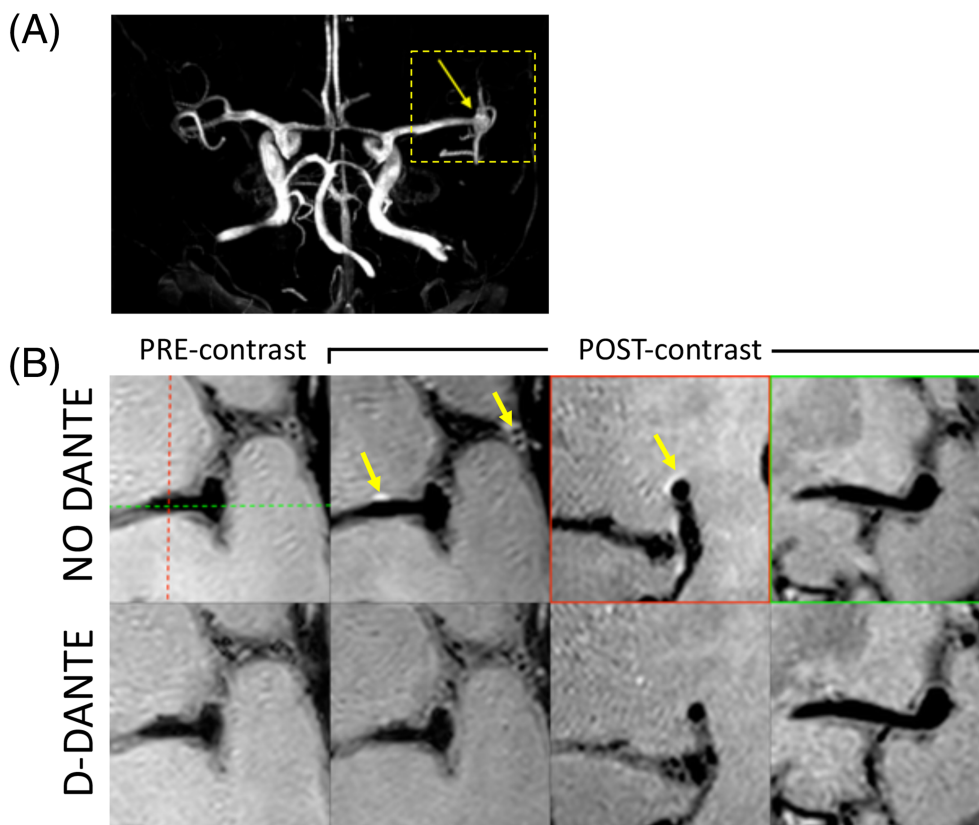


FIGURE 5 Feasibility of D-DANTE in a patient with an intracranial aneurysm. (A) MR angiography scan indicating the location of the intracranial aneurysm at the M1/M2 junction. (B) Precontrast and postcontrast imaging using regular 3D turbo spin echo (TSE) or D-DANTE-prepared 3D TSE. Contrast enhancement around the middle cerebral artery (MCA) was only seen for regular 3D TSE and was proven to originate from a crossing vein, mostly likely due to unsuppressed slow flow. DANTE, delay alternating with nutation for tailored excitation; D-DANTE, Double DANTE

further optimized to facilitate imaging at such high resolutions. Again, we would like to highlight that because D-DANTE merely changes the specific phase evolution of the DANTE RF pulse train, we used optimized parameters from the literature²¹ and focused on a direct comparison of the two sequences.

SNR and CNR values for regular DANTE as measured in this study were very similar to previous studies at 3T.^{21,32} A study performed at 7T by Viessmann et al.¹⁰ reported much higher SNR values in VW tissue, although VW/CSF contrast was only moderately higher than that reported here. This could indicate that CSF suppression using DANTE is slightly compromised by B1 inhomogeneities, which are common at field strengths above 3T. Also, the use of 7T comes with slightly less favorable T1 values (less relaxation between shots and more saturation during DANTE preparation) and T2 values (more relaxation during 3D TSE readout), but the gain in SNR should compensate for this sufficiently. These positive experiences regarding the use of DANTE at 7T would, in our view, be directly applicable to D-DANTE as well and would facilitate IC-VWI at even higher resolutions than reported here. In our comparison between D-DANTE and regular DANTE, we did not perform registration between repeated scans. Instead, visual inspection of ROIs in repeated scans ensured that the same ROIs were chosen with no significant difference in the number of voxels for both methods (data not shown).

As in our patient example, IC-VWI is often performed precontrast and postcontrast as a marker of VW inflammation.^{2,33} In this study, we did not systematically assess the performance of contrast-enhanced D-DANTE imaging, although we believe this would perform equally well as for regular DANTE, as shown by others in the literature.^{8,34,35} From our patient case included in this study, we indeed observed that (D-)DANTE might be more robust to suppress slow-flow artifacts compared with regular 3D TSE sequences, especially for postcontrast scans. This is of interest, because others have stressed the importance of adequate slow flow suppression to prevent misdiagnosis due to apparent VW enhancement.³⁶ Another important aspect for postcontrast imaging is to achieve proper T1 weighting of the signal. For this purpose, note that because of the DANTE preparation, TR needs to be prolonged to achieve similar T1-weighting compared with regular 3D TSE sequences.

A limitation of the method as performed in this study is that to keep acquisition times within an acceptable range of 4–6 min, only one signal average was used, which gave rise to TSE-related free induction decay (FID) artifacts.³⁷ Although DANTE artifacts and FID artifacts have a similar appearance, the latter present themselves locally and strongly depend on the underlying tissue characteristics, whereas DANTE artifacts appear

as structured bands across the entire FOV. In theory, the use of two averages in combination with phase-cycling would eliminate the FID artifact, however, this would require an additional doubling of the SENSE acceleration, compromising SNR efficiency as a result of g-factor noise. However, as an alternative (see also Figure S2), we were able to show that the use of two averages in combination with four times the acceleration using compressed sensing³⁸ provided images of good quality without the presence of FID artifacts. Instead of using two signal averages, one can also prevent the occurrence of FID artifacts by increasing the echo spacing during TSE readout. However, this lengthens the readout and reduces the effective T1 relaxation during TR, and possibly the SNR efficiency of the sequence. Finally, D-DANTE was only evaluated for $\Delta\Phi = 22.5^\circ$ in the in vivo experiments as this value provided the most homogenous distribution of signal bands and better SNR compared with the $\Delta\Phi = 180^\circ$ case. The latter could, of course, become valuable in cases when even higher resolution imaging than presented here is required.

5 | CONCLUSION

D-DANTE can provide banding artifact-free IC-VWI up to higher isotropic resolutions compared with regular DANTE, however, with a modest reduction in VW SNR. This allows for more a flexible choice of DANTE preparation parameters in IC-VWI applications.

ACKNOWLEDGEMENTS

We would like to thank Linqing Li for his useful feedback on the final manuscript. Also, we would like to acknowledge Eva Leemans for helping to set up the acquisition of the patient dataset as part of a clinical research examination. BFC received funding from the Dutch Research Council (NWO Veni grant 14348).

DATA AVAILABILITY STATEMENT

The data that support the findings of this study are available from the corresponding author upon reasonable request.

ORCID

Jaco J. M. Zwanenburg  <https://orcid.org/0000-0002-4282-5719>

Jeroen C. W. Siero  <https://orcid.org/0000-0001-5079-2868>

REFERENCES

- Lindenholz A, van der Kolk AG, Zwanenburg JJM, Hendrikse J. The use and pitfalls of intracranial vessel wall imaging: How we do it. *Radiology*. 2018; 286(1):12-28.
- Mandell DM, Mossa-Basha M, Qiao Y, et al. Intracranial vessel wall MRI: Principles and expert consensus recommendations of the American Society of Neuroradiology. *Am J Neuroradiol*. 2017;38(2):218-229.
- Hartevelde AA, van der Kolk AG, van der Worp HB, et al. High-resolution intracranial vessel wall MRI in an elderly asymptomatic population: comparison of 3T and 7T. *Eur Radiol*. 2017;27(4):1585-1595.
- Wang J, Yarnykh VL, Hatsukami T, Chu B, Balu N, Yuan C. Improved suppression of plaque-mimicking artifacts in black-blood carotid atherosclerosis imaging using a multislice motion-sensitized driven-equilibrium (MSDE) turbo spin-echo (TSE) sequence. *Magn Reson Med*. 2007;58(5):973-981.
- Li L, Miller KL, Jezzard P. DANTE-prepared pulse trains: A novel approach to motion-sensitized and motion-suppressed quantitative magnetic resonance imaging. *Magn Reson Med*. 2012;68(5):1423-1438.
- Zhang Z, Fan Z, Carroll TJ, et al. Three-dimensional T2-weighted MRI of the human femoral arterial vessel wall at 3.0 Tesla. *Invest Radiol*. 2009;44(9): 619-626.
- Zhu C, Haraldsson H, Faraji F, et al. Isotropic 3D black blood MRI of abdominal aortic aneurysm wall and intraluminal thrombus. *Magn Reson Imaging*. 2016;34(1):18-25.
- Xie Y, Yang Q, Xie G, Pang J, Fan Z, Li D. Improved black-blood imaging using DANTE-SPACE for simultaneous carotid and intracranial vessel wall evaluation. *Magn Reson Med*. 2016;75(6):2286-2294.
- Wang J, Helle M, Zhou Z, Börner P, Hatsukami TS, Yuan C. Joint blood and cerebrospinal fluid suppression for intracranial vessel wall MRI. *Magn Reson Med*. 2016;75(2):831-838.
- Viessmann O, Li L, Benjamin P, Jezzard P. T2-weighted intracranial vessel wall imaging at 7 Tesla using a DANTE-prepared variable flip angle turbo spin echo readout (DANTE-SPACE). *Magn Reson Med*. 2017;77(2):655-663.
- Scheffler K, Lehnhardt S. Principles and applications of balanced SSFP techniques. *Eur Radiol*. 2003;13(11):2409-2418.
- Axel L, Dougherty L. Heart wall motion: improved method of spatial modulation of magnetization for MR imaging. *Radiology*. 1989;172(2):349-350.
- Geen H, Wu X-L, Xu P, Friedrich J, Freeman R. Selective excitation at two arbitrary frequencies. The double-DANTE sequence. *J Magn Reson*. 1989; 81(3):646-652.
- Bernstein MA, King KF, Zhou XJ. *Handbook of MRI Pulse Sequences*. Elsevier; 2004.
- Spijkerman JM, Petersen ET, Hendrikse J, Luijten P, Zwanenburg JJM. T2 mapping of cerebrospinal fluid: 3 T versus 7 T. *Magn Reson Mater Phys Biol Med*. 2018;31(3):415-424.
- Coolen BF, Poot DHJ, Liem MI, et al. Three-dimensional quantitative T1 and T2 mapping of the carotid artery: Sequence design and in vivo feasibility. *Magn Reson Med*. 2016;75(3):1008-1017.
- Biasioli L, Lindsay AC, Chai JT, Choudhury RP, Robson MD. In-vivo quantitative T2 mapping of carotid arteries in atherosclerotic patients: segmentation and T2 measurement of plaque components. *J Cardiovasc Magn Reson*. 2013;15(1):69.

18. Koning W, de Rotte AAJ, Bluemink JJ, et al. MRI of the carotid artery at 7 Tesla: Quantitative comparison with 3 Tesla. *J Magn Reson Imaging*. 2015;41(3):773-780.
19. Qin Q. A simple approach for three-dimensional mapping of baseline cerebrospinal fluid volume fraction. *Magn Reson Med*. 2011;65(2):385-391.
20. Qi H, Sun J, Qiao H, et al. Simultaneous T1 and T2 mapping of the carotid plaque (SIMPLE) with T2 and inversion recovery prepared 3D radial imaging. *Magn Reson Med*. 2018;80(6):2598-2608.
21. Cogswell PM, Siero JCW, Lants SK, et al. Variable impact of CSF flow suppression on quantitative 3.0T intracranial vessel wall measurements. *J Magn Reson Imaging*. 2018;48(4):1120-1128.
22. Yushkevich PA, Piven J, Hazlett HC, et al. User-guided 3D active contour segmentation of anatomical structures: Significantly improved efficiency and reliability. *Neuroimage*. 2006;31(3):1116-1128.
23. Kellman P, McVeigh ER. Image reconstruction in SNR units: A general method for SNR measurement. *Magn Reson Med*. 2005;54(6):1439-1447.
24. Brown RW, Cheng YCN, Haacke EM, Thompson MR, Venkatesan R. *Magnetic Resonance Imaging: Physical Principles and Sequence Design*. Second ed. New York: John Wiley And Sons, Inc.; 2014.
25. Qu J, Lin T, Wei X, Wu B, Feng F. Banding free DANTE prepared vessel wall imaging incorporating multiple acquisition and phase cycling. In: *Proceedings of the Annual Meeting ISMRM*; 2018:1891.
26. Jia S, Zhang L, Ren L, et al. Joint intracranial and carotid vessel wall imaging in 5 minutes using compressed sensing accelerated DANTE-SPACE. *Eur Radiol*. 2020;30(1):119-127.
27. Li L, Chai JT, Biasioli L, et al. Black-blood multicontrast imaging of carotid arteries with DANTE-prepared 2D and 3D MR imaging. *Radiology*. 2014;273(2):560-569.
28. Qiao Y, Steinman DA, Qin Q, et al. Intracranial arterial wall imaging using three-dimensional high isotropic resolution black blood MRI at 3.0 Tesla. *J Magn Reson Imaging*. 2011;34(1):22-30.
29. Zhang L, Zhang N, Wu J, et al. High resolution three dimensional intracranial arterial wall imaging at 3 T using T1 weighted SPACE. *Magn Reson Imaging*. 2015;33(9):1026-1034.
30. Yang H, Zhang X, Qin Q, Liu L, Wasserman BA, Qiao Y. Improved cerebrospinal fluid suppression for intracranial vessel wall MRI. *J Magn Reson Imaging*. 2016;44(3):665-672.
31. Fan Z, Yang Q, Deng Z, et al. Whole-brain intracranial vessel wall imaging at 3 Tesla using cerebrospinal fluid-attenuated T1-weighted 3D turbo spin echo. *Magn Reson Med*. 2017;77(3):1142-1150.
32. Zhang L, Zhang N, Wu J, Liu X, Chung Y-C. High resolution simultaneous imaging of intracranial and extracranial arterial wall with improved cerebrospinal fluid suppression. *Magn Reson Imaging*. 2017;44:65-71.
33. Hartman JB, Watase H, Sun J, et al. Intracranial aneurysms at higher clinical risk for rupture demonstrate increased wall enhancement and thinning on multicontrast 3D vessel wall MRI. *Br J Radiol*. 2019;92(1096):20180950.
34. Tsubouchi R, Ohira J, Sawamura M, et al. Multiple cranial neuritis depicted with DANTE-prepared contrast-enhanced MRI. *Neurol Clin Neurosci*. 2020;8(4):220-221.
35. Komatsu K, Takagi Y, Ishii A, et al. Ruptured intracranial aneurysm of an arteriovenous malformation diagnosed by delay alternating with nutation for tailored excitation (DANTE)-prepared contrast-enhanced magnetic resonance imaging. *Acta Neurochir*. 2018;160(12):2435-2438.
36. Cornelissen BMW, Leemans EL, Coolen BF, et al. Insufficient slow-flow suppression mimicking aneurysm wall enhancement in magnetic resonance vessel wall imaging: a phantom study. *Neurosurg Focus*. 2019;47(1):E19.
37. Mugler JP. Optimized three-dimensional fast-spin-echo MRI. *J Magn Reson Imaging*. 2014;39(4):745-767.
38. Lustig M, Donoho D, Pauly JM. Sparse MRI: The application of compressed sensing for rapid MR imaging. *Magn Reson Med*. 2007;58(6):1182-1195.

SUPPORTING INFORMATION

Additional supporting information may be found online in the Supporting Information section at the end of this article.

How to cite this article: Coolen BF, Schoormans J, Gilbert G, et al. Double delay alternating with nutation for tailored excitation facilitates banding-free isotropic high-resolution intracranial vessel wall imaging. *NMR in Biomedicine*. 2021;34:e4567. <https://doi.org/10.1002/nbm.4567>